UCRL-10267

University of California

Ernest O. Lawrence Radiation Laboratory

NEUTRON DEPTH DOSE FROM (α, n) AND (γ, n) SOURCES IN A TISSUE-EQUIVALENT PHANTOM

Berkeley, California

DISCLAIMER

UCRL-10267
UC-41 Health & Safety
TID-4500 (19th Ed.)

UNIVERSITY OF CALIFORNIA

Lawrence Radiation Laboratory
Berkeley, California

Contract No. W-7405-eng-48

NEUTRON DEPTH DOSE FROM (α, n) AND (γ, n) SOURCES IN A TISSUE-EQUIVALENT PHANTOM

Henry Aceto, Jr. and Bruce W. Churchill

March 4, 1963

Printed in USA. Price 75 cents. Available from the
Office of Technical Services
U. S. Department of Commerce
Washington 25, D.C.

NEUTRON DEPTH DOSE FROM (α, n) AND (γ, n) SOURCES IN A TISSUE-EQUIVALENT PHANTOM

Henry Aceto, Jr. and Bruce W. Churchill

Lawrence Radiation Laboratory
University of California
Berkeley, California

March 4, 1963

ABSTRACT

Neutron depth-dose behavior in tissue-equivalent phantom exposed to SbBe, PoLi, Po mock fission, and PuBe point sources has been examined with respect to existing theoretical and experimental calculations. Dose from exposure to a point source of complex energy spectra can be estimated by applying a $1/r^2$ geometric correction to the incident neutron flux and comparing the result with the known monoenergetic behavior of neutrons equivalent to the average energy of the point source neutrons.

NEUTRON DEPTH DOSE FROM (α, n) AND (γ, n) SOURCES IN A TISSUE-EQUIVALENT PHANTOM

Henry Aceto, Jr.* and Bruce W. Churchill

Lawrence Radiation Laboratory
University of California
Berkeley, California

March 4, 1963

I. INTRODUCTION

The object of this study is to experimentally determine the dose delivered as a function of depth into a human phantom by various point neutron sources of different energy spectra.

Fast neutrons incident on tissue lose their energy primarily by elastic scattering collisions with tissue nuclei, the lost energy being transferred to the scattered nucleus. The nucleus in turn dissipates its acquired kinetic energy by ionization, excitation, and elastic collisions with other atoms in the tissue. Inelastic scattering does occur for neutron energies above a few MeV with a cross section increasing with energy, but for neutrons with energies below 10 MeV, the interval of primary concern, inelastic scattering is unimportant. Hydrogen collisions predominate, none of which are inelastic, and in such collisions as do occur with heavier nuclei the emitted gamma photon, on the average, is a small fraction of the energy carried by the recoil atom.

The average fraction F of the energy lost by the neutron per elastic collision is dependent only on the mass of the target nucleus.[1] The average energy of neutrons of energy E_0 undergoing an elastic collision is given by

$$\bar{E} = E_0 \left[1 - \frac{2A}{(A+1)^2}\right] ,$$

where A is the mass number of the target nucleus.

This leads to an expression for the average energy after n collisions, with hydrogen,

$$\bar{E}_n = \left(\frac{1}{2}\right)^n E_0 ,$$

which is misleading since most of the neutrons will have a much smaller energy; i.e., the median energy is less than the average energy. Consequently

---

* Present address: University of Texas, Southwestern Medical School, Dept. of Radiology, Dallas, Texas.

the number of collisions n needed to reduce a neutron to a given energy is best calculated by using logarithmic energy decrements as set forth by Fermi:

$$E_n \approx E_0 e^{-n\xi} \quad , \quad \xi = \overline{\ln \frac{E_j}{E_{j+1}}} = 1 - \frac{(A-1)^2}{2A} \ln\left(\frac{A+1}{A-1}\right) \quad ,$$

where ξ is the average logarithmic energy decrease per elastic collision—again dependent only on the mass of the target nuclei—and E_n is the median energy after n collisions. However, the range of a charged recoil nucleus in tissue is small and, because we are interested in its deposition of energy near the site of collision rather than the number of collisions necessary to thermalize the neutron, the average energy loss fraction $F = 2A/(A+1)^2$ will be assumed in the calculations. Thus the lighter atoms, particularly hydrogen, are most effective in dissipating the neutron energy. The average fraction of energy lost in collisions with hydrogen is 0.5, compared with 0.142 for carbon, 0.124 for nitrogen, and 0.111 for oxygen. From Table I one can readily see that the ratio of moderating power $\xi_H N_H \sigma_H$ of hydrogen in tissue to the total moderating power $\Sigma_i \xi_i N_i \sigma_i$ of all nuclei composing tissue does not suggest a significant contribution from the other nuclei. Tochilin and Ross[2] estimate the energy transferred to tissue by first-collision hydrogen scattering to be approximately 90% of the total energy loss by fast neutrons.

Table I. Neutron scattering properties.

Element	Mass No.	ξ[a]	Neutron energy (MeV)	$\frac{\xi_H N_H \sigma_H}{\xi_i N_i \sigma_i}$
H	1	1.000	0.030	0.985
C	12	0.158	0.460	0.988
N	14	0.136	1.6	0.935
O	16	0.120	4.2	0.926

[a] $\xi = \ln \frac{E_0}{E_1} = 1 + \frac{(A-1)^2}{2A} \ln \frac{A-1}{A+1}$

A certain fraction of the incident neutrons will be moderated in the body and absorbed at thermal energies; the products of the nuclear reactions contribute to the dose. The predominant reactions are $H^1(n, \gamma)H^2$, which yields a 2.2-MeV gamma photon; $N^{14}(n, p)C^{14}$, which yields a 0.63-MeV proton; and $N^{14}(n, \gamma)N^{15}$, which yields an energy of 10.8 MeV. Although the cross section for the $N^{14}(n, \gamma)N^{15}$ is significant at thermal energies, its contribution to the quanta energy is about 5% of the capture gamma energy of hydrogen.[3] Furthermore, since the gamma absorption cross section decreases with increasing energy,* it can be assumed that this reaction constitutes less

* In water, the ratio of the absorption coefficient of 2.2-MeV photons to that of 10.8-MeV photons is approximately 1.6.

than 5% of the overall gamma dose resulting from thermal capture.[3] The 0.63-MeV proton from the nitrogen-capture reaction loses its energy within microns of the reaction site, and the dose delivered at any point in the phantom may be computed directly from the collision density at that point. In contrast, the gamma quanta originating from hydrogen capture will deliver their energy within a large volume of tissue surrounding the collision site.

In view of the above considerations, the reactions considered in this study as the primary sources of tissue energy absorption are elastic collisions of fast neutrons on hydrogen and the thermal reactions $N^{14}(n, p)C^{14}$ and $H^{1}(n, \gamma)D^{2}$.

In 1954 Snyder and Neufeld first calculated the depth distribution of fast-neutron doses by using collision histories estimated statistically with the Monte Carlo method.[6] The calculations were applied to beams of monoenergetic neutrons incident normally on an infinite slab of tissue 30 cm thick. Kogan et al.,[3] in 1959, imposed similar conditions and calculated the dose distribution by a numerical solution of the kinetic Boltzman equation. In 1961 Smith and Boot[7] undertook an experimental confirmation of the above calculations by using a man-equivalent phantom and various sources primarily chosen to simulate broad-beam monoenergetic conditions. In general they produced satisfactory agreement between theory and experimentation. The present work, which employs a phantom similar to that used by Smith and Boot, is primarily concerned with point sources of complex energy spectra.

II. EXPERIMENTAL METHOD

A. Phantom

The human body was simulated by an elliptically shaped right cylinder, 20 by 36 cm by 60 cm high, made of 0.65-cm polyethylene. Neutron flux measurements were made with the phantom filled with tissue-equivalent fluid and with water (Table II). A wooden stand supported the phantom 130 cm above the ground (Fig. 1). Figure 2 indicates that scattering from the ground is at a minimum under these conditions. The experiment was conducted outdoors, thus eliminating any scattering contributions from walls.

B. Neutron Sources

Three (α, n) sources with quite different neutron spectra and a photoneutron source served as the source of neutrons. The actual spectra of most radioactive sources has been variously reported by different investigators. For purposes of this paper, 30 keV was accepted as the mean energy of the SbBe photoneutron source; the PoLi, Po mock fission, and PuBe mean energies were considered to be 0.46, 1.6, and 4.2 MeV, respectively.

The source was placed normal to the front surface of the phantom, thus making inverse-square corrections of the incident flux necessary. Figure 3 indicates the breakdown of inverse square at small source-detector distances.

Table II. Tissue-equivalent-fluid composition.

	Percent by weight
Urea	8.57
Sucrose	22.58
Water	67.85
o-cresol	1.00

Element	Percent by weight	Atomic density[a] $\times 10^{22}$ cm^{-3}	Average wet tissue percent by weight
Oxygen	74	2.784	74
Carbon	12	0.602	12
Hydrogen	10	5.98	10
Nitrogen	4	0.172	4

[a] Assuming density of tissue is 1.00.

C. Method

Figure 4 shows a block diagram of the associated electronic equipment. Fast-neutron energy measurements were made with a polyethylene-lined proportional counter filled with different gases. The counter was enclosed in a 1/32-in. -thick lucite holder (see Figs. 5 and 6). The size of the counter used for these particular measurements most certainly causes some perturbation of the field, although the correction is probably only a few percent, with the maximum effect occurring for measurements taken at or near the surface of the phantom.[4] The effect of the holder on the readings was checked and found to be negligible. The counter was made gamma insensitive by appropriate choice of discriminator setting, and was periodically checked with a radium source of known gamma strength. The polyethylene liner was 1/8 in. thick. It is important that the polyethylene liner be thicker than the range of the most energetic recoil protons, but not thick enough to produce appreciable attenuation of the fast neutrons.[5] As shown by Moyer,[5] under these conditions the counter will measure the energy flux in MeV/cm^2 carried by the fast neutrons; the response is proportional to the flux.

Because the ranges of the recoil protons from the elastic scattering of the fast neutrons are quite small (on the order of microns), the final deposition of energy will be distributed essentially according to the collision density weighted by the neutron energy. Lehman inferred mean neutron energies from the PuBe source at various depths in a phantom directly from the recoil proton spectrum yielded by the track density and lengths recorded on exposed nuclear emulsions.[8] The experimental dose due to fast neutrons is proportional to the energy flux measured by polyethylene proportional counters and the scattering cross sections corresponding to the neutron energies determined by the emulsions.

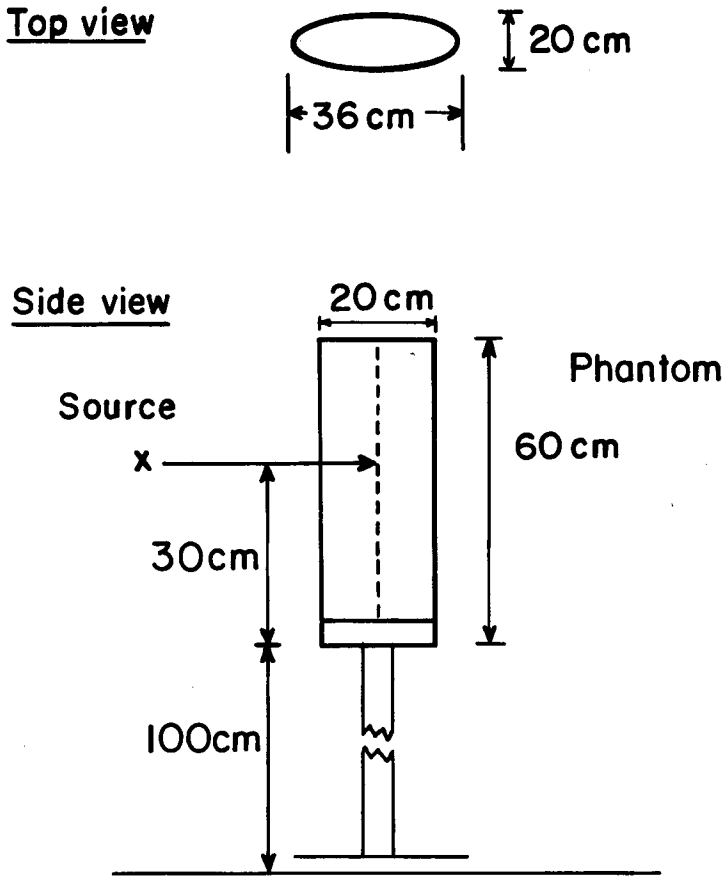

Fig. 1. Phantom dimensions and position.

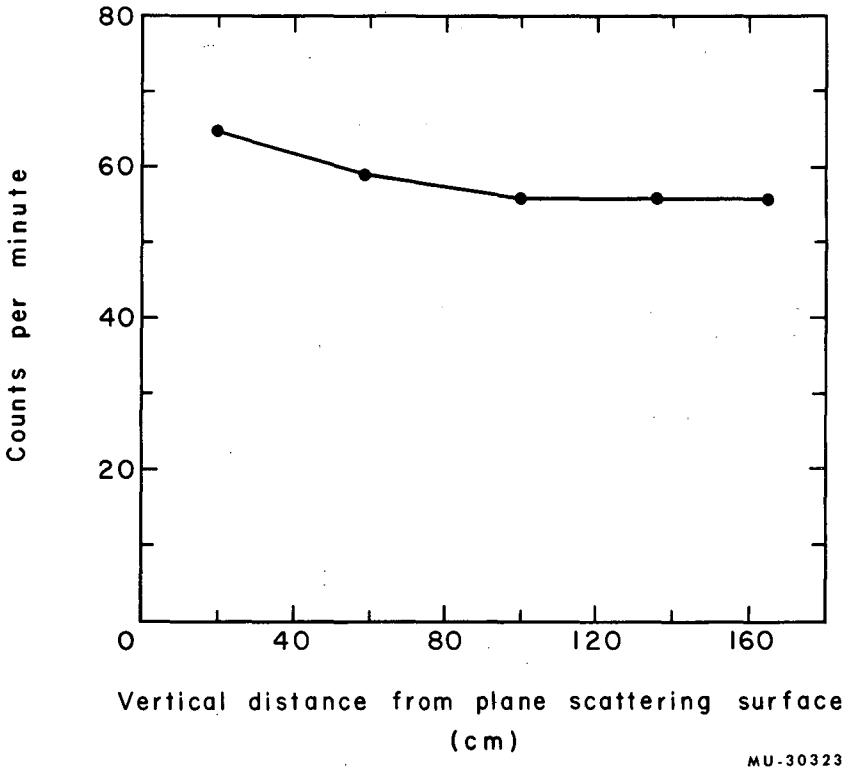

Fig. 2. Ground scattering as a function of height.

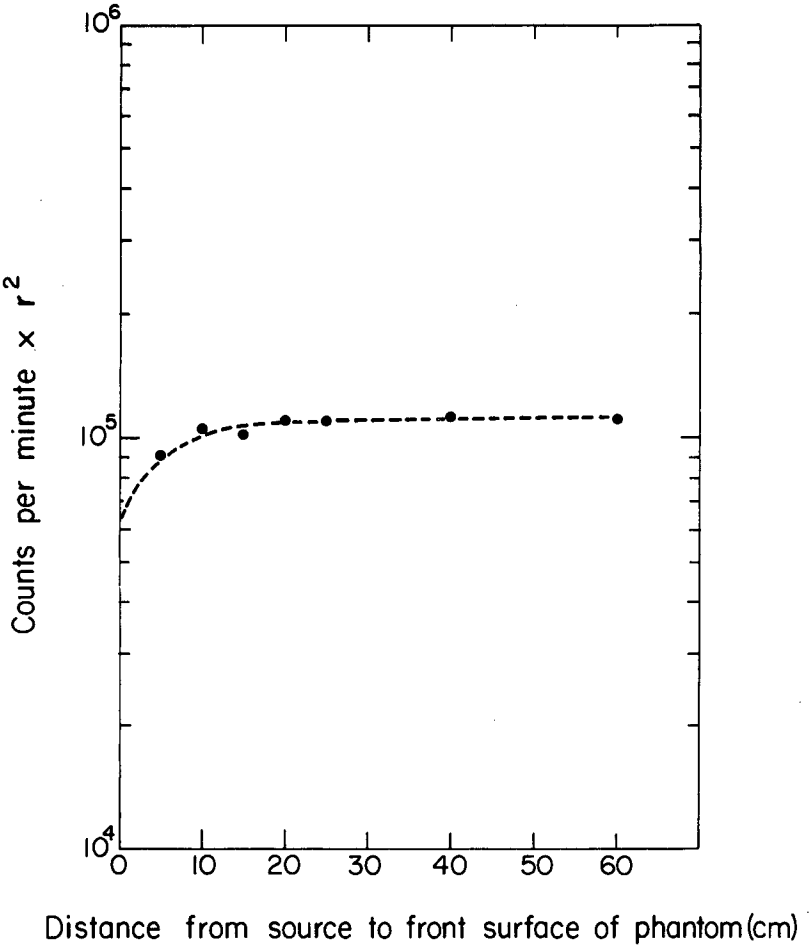

Fig. 3. Inverse square reliability as a function of distance.

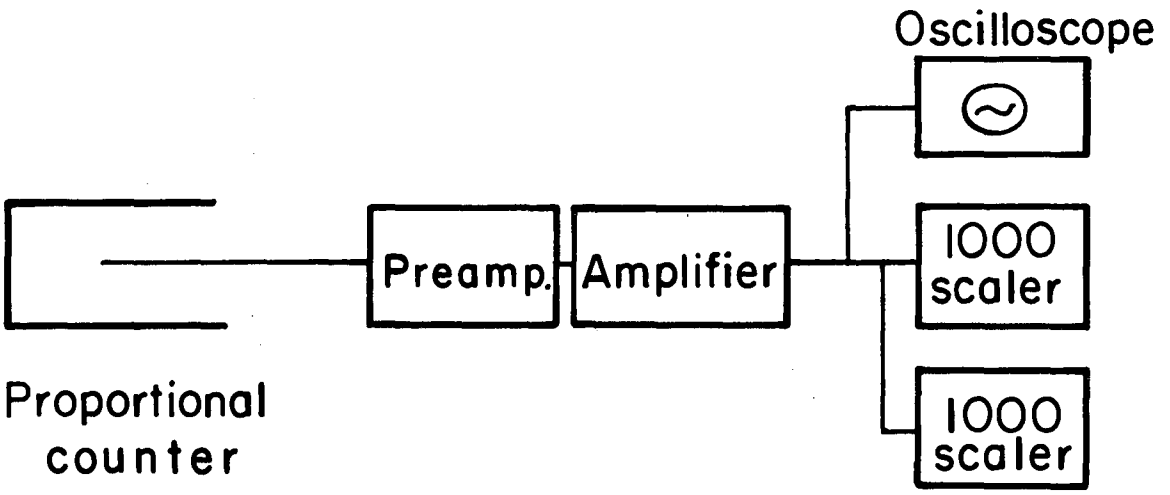

Fig. 4. Block diagram of associated electronic equipment.

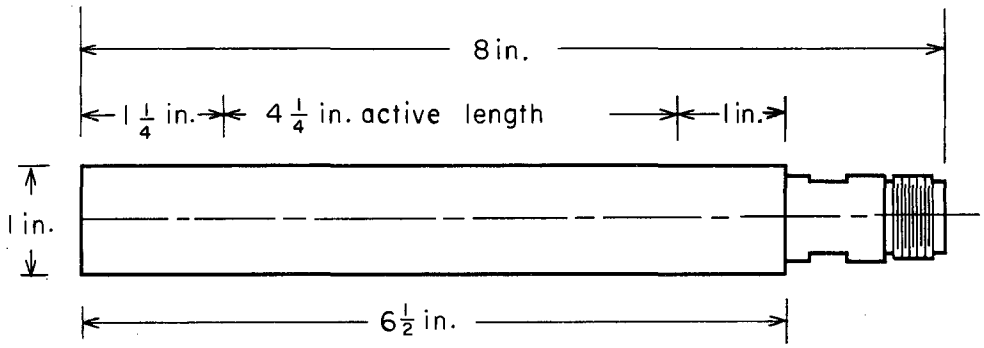

Body material 1100 aluminum

1/8 inch thick polethylene liner

Fill gas	Pressure (cm of Hg)
BF_3 (B^{10} enriched)	60
Ethylene	76

MU-27032

Fig. 5. Proportional counter.

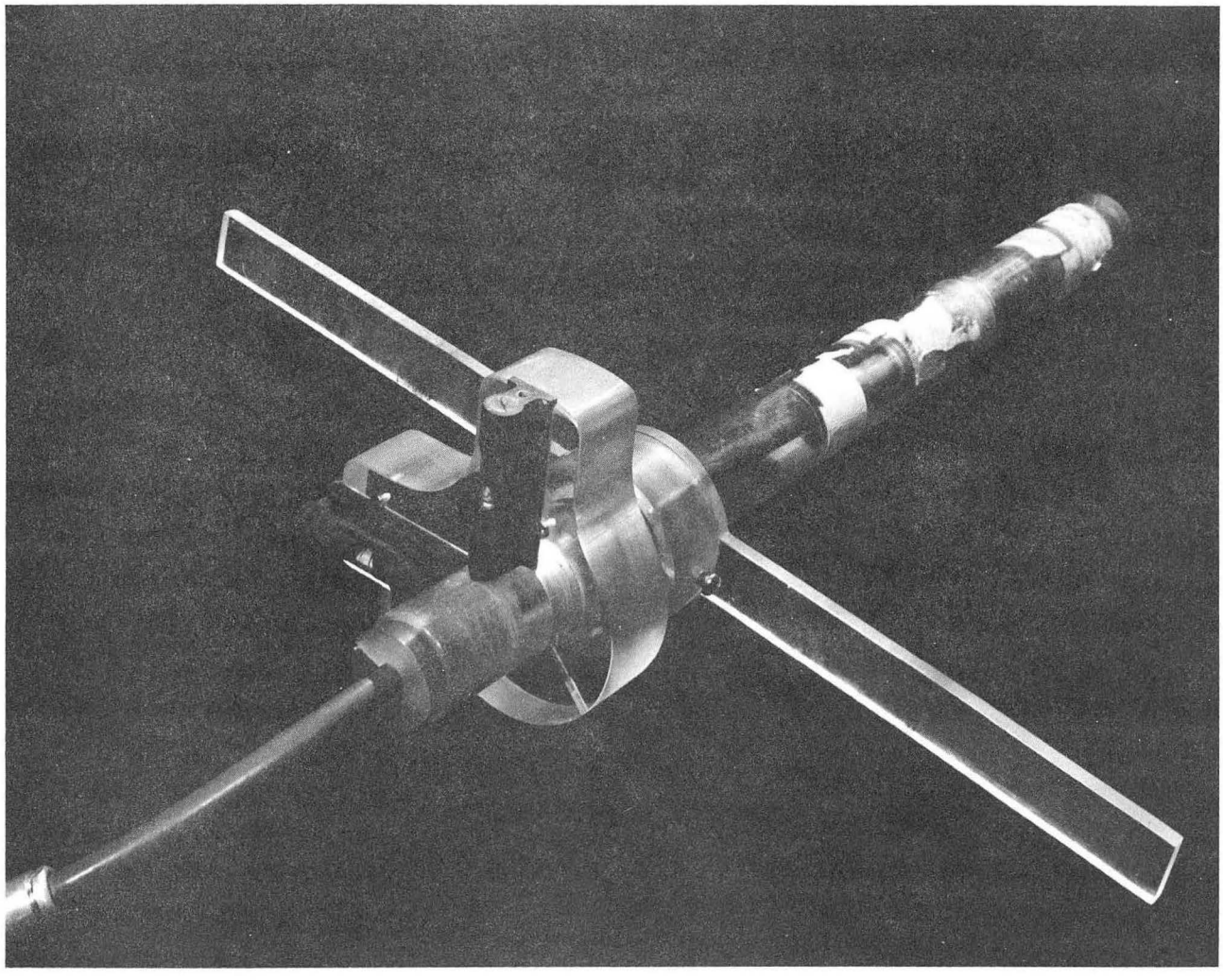

ZN-3692

Fig. 6. Lucite holder for proportional counters.

The slow-neutron flux was measured by thin circular indium foils, each mounted on thin lucite backing. The foils, approximately 2.5 cm in diameter, were mounted normal to the source and to the front surface of the phantom on rigid lucite strips fastened at the top and bottom of the phantom. Comparison of multi-foil and single-foil exposures indicated that the foils suffered a flux depression of about 5% due to the proximity of neighboring foils. The flux depression by the lucite strips was not found to be of great significance and was neglected. The flux-depression factor due to the introduction of the foils into the unperturbated field[9] was calculated and found to be 1.15; i.e., the neutron density was depressed 0.15/1.15 or 13% by the presence of the 92-mg/cm^2 indium foils (Appendix A).

The calibrations of the slow-neutron detectors were made by using the slow-neutron flux created by a fast-neutron source placed in a concrete cavity. From the strength of the fast-neutron source, the thermal-neutron flux within the cavity may be estimated, independent of the source spectrum:

$$\text{thermal flux} = 1.25\ Q/S,$$

where Q is the source strength in neutrons/sec and S is the inner surface area of the cavity.[10] Because of the 1/v dependence of the indium cross section and the high resonance peak at 1.5 eV, the calibrations would be accurate only if the thermal-epithermal spectrum in the cavity were the same as the corresponding spectral region within the phantom. Since the shape of the thermal spectrum within the phantom varies with depth into the phantom, an actual correspondence between phantom and cavity does not exist. In order to better interpret the neutron fluxes measured by foils calibrated in this manner, an attempt was made to compare the thermal spectrum of the cavity to that at various depths within the phantom (Appendix B). This comparison, by means of measurements with bare and Cd-covered indium foils in the cavity and the phantom, indicates that the final dose results would be minimal.

All foil measurements in the phantom for dose calculation were compared to BF_3 counter-measurements under identical conditions. The comparison showed very close agreement.

III. RESULTS

A. Fast Neutrons

The calculation of fast-neutron absorbed dose will rest on the reasonable assumption that consideration of the proton recoil component of the dose alone will yield sufficiently accurate results. Consequently, the energy-flux field intensity measurements together with the macroscopic cross section for hydrogen corresponding to the mean neutron energy at a point in the phantom will give the energy transferred per volume element at that point. If we assume (a) that on the average half of the incident-neutron energy is transferred to the recoil proton per collision and (b) that the resultant energy absorbed per volume element originated from the elastic collision within that volume element (provided the change in energy flux over the distance represented by the range of the recoil protons is small), and if we know the energy spectrum of the neutrons at the point in question, we may quite readily determine the absorbed dose at that point:

$$\text{rads} = \left[\text{MeV/cm}^2\right]\left[N_H \sigma_H \text{cm}^{-1}\right]\left[8\times10^{-9}\right] .$$

The resultant depth-dose curve for PuBe neutrons as shown by Fig. 7 agrees fairly well with the proton dose of Snyder. The dose to the back of the phantom appears to be approximately 16% of the dose to the front, with a relaxation length of 8.5 cm. The main difference between the two studies, aside from the source types, is in the models used to simulate the human body. In addition, Snyder's curves represent the energy absorption resulting from recoil protons, and of the protons produced by the (n, p) reaction averaged together. This study has separated the two.

Fast-neutron dose measurements in tissue-equivalent fluid and water are compared in Fig. 8. The depth-dose curves in tissue-equivalent fluid and water, all other conditions being the same, show little difference within the statistical limitations imposed by the experimental conditions. This is not surprising since the tissue-equivalent fluid and water differ by approximately 1% in their atomic densities for hydrogen. Also, the greatest difference between the energy absorbed by molecules of water and TE fluid per unit numerical flux density is only 3% when their complete atomic composition is considered (Fig. 9).

The fast-neutron dose may be calculated by use of the emulsions alone. A count of the emulsion track density, yielding recoil protons/cm^2, multiplied by the average proton energy will yield a dose figure in energy absorbed per unit volume. Figure 10 shows Lehman's absolute track densities corrected to broad-beam conditions.[8] By computer analysis the average energy of the proton recoils was found by calculating

$$\frac{\Sigma\frac{\Delta N}{P\Delta E}\cdot E\Delta E}{\Sigma\frac{\Delta N}{P\Delta E}\cdot \Delta E}$$

for the Ilford film, where ΔN is the number of tracks in the energy interval ΔE, and P is the geometry correction factor.[8]

The mean recoil-proton energy—excluding thermal n, p tracks—for PuBe neutrons was found by Lehman to vary from 1.26 to 1.57 MeV at different depths in the phantom (Fig. 11). This low proton spectral range is primarily due to the presence of low-energy secondary collision neutrons. Comparison with Fig. 12 indicates that the $\bar{E}$ minimum corresponds roughly with the position of the maximum concentration of thermal neutrons from the PuBe source. The average recoil proton energy then increases with depth, corresponding to a simultaneous decrease of the thermal population.

The emulsion dose calculated by the product of the track density and the average recoil proton energy (Fig. 7) has its largest disagreement with the proportional-counter results and with Snyder's results at the front

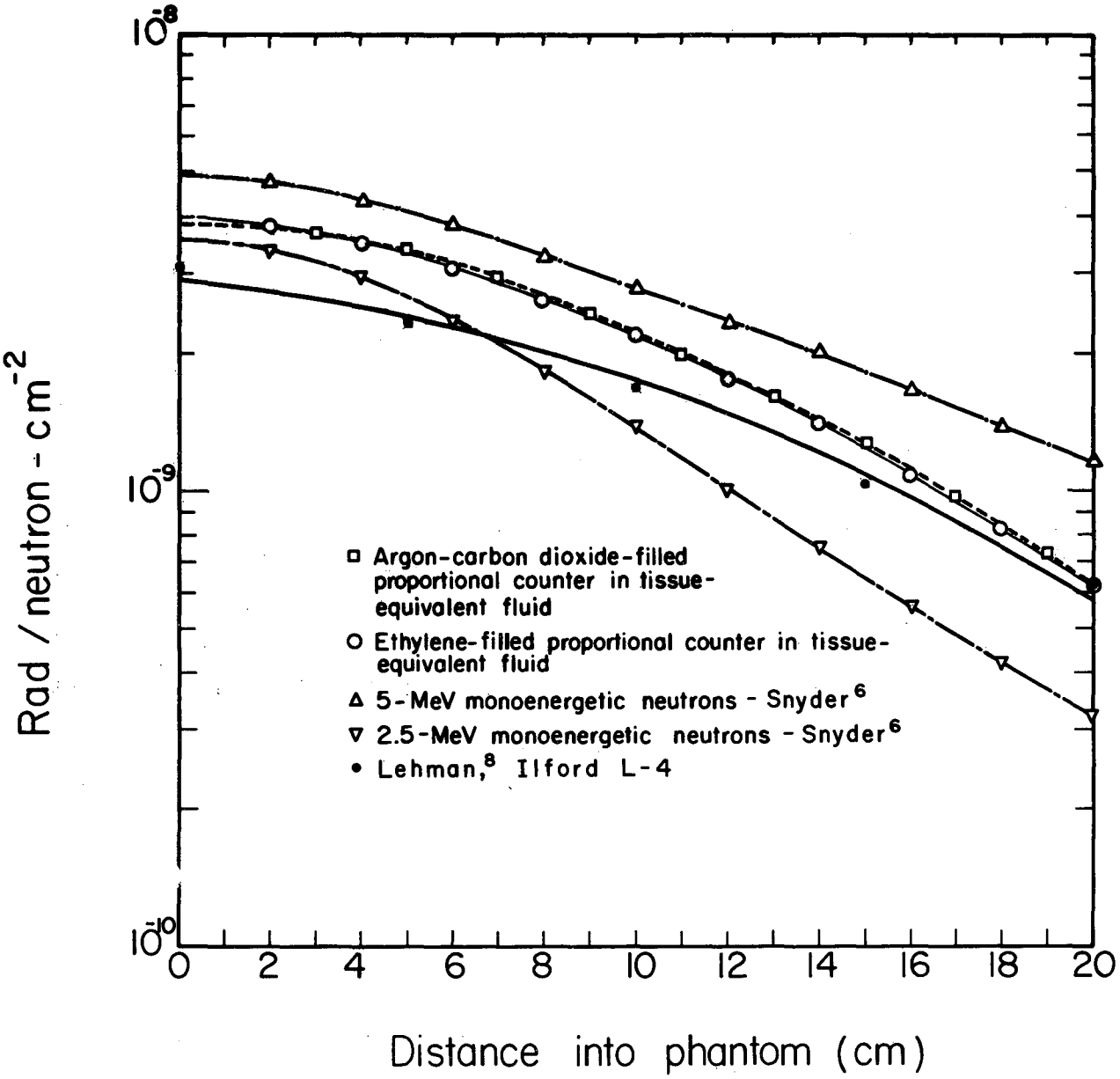

Fig. 7. Fast-neutron depth-dose curve for PuBe neutrons.

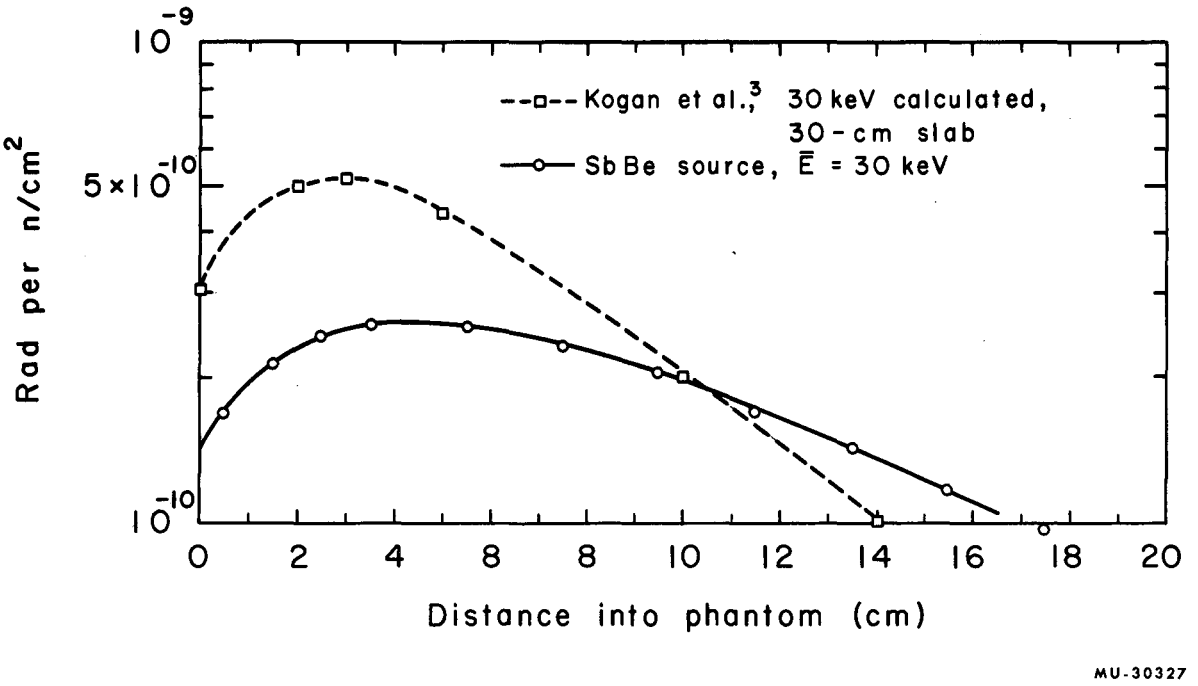

Fig. 8. Comparison of dose measurements in water and tissue-equivalent fluid.

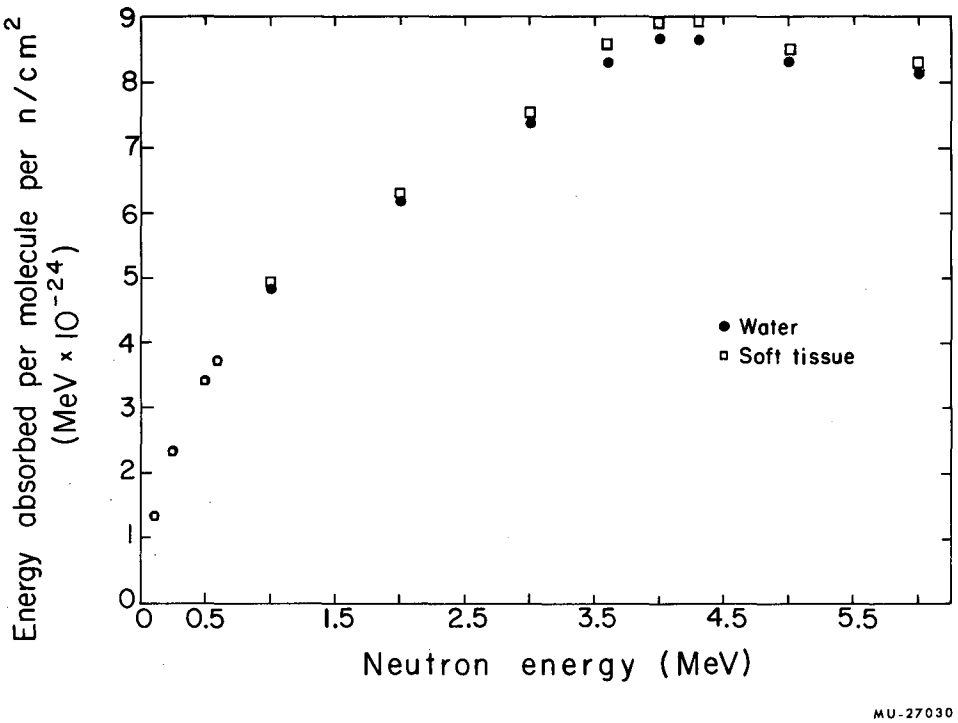

Fig. 9. Comparison of molecular energy absorption in water and tissue-equivalent fluid.

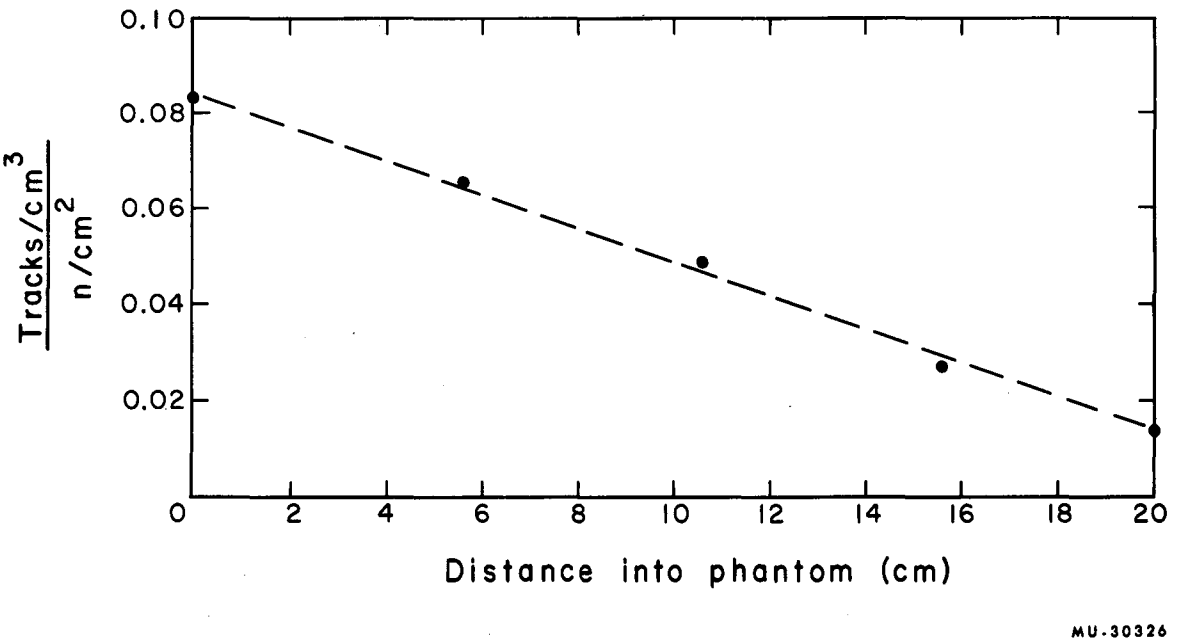

Fig. 10. Recoil proton track density per incident neutron with depth in Phantom corrected for $1/r^2$ (Lehman[8]).

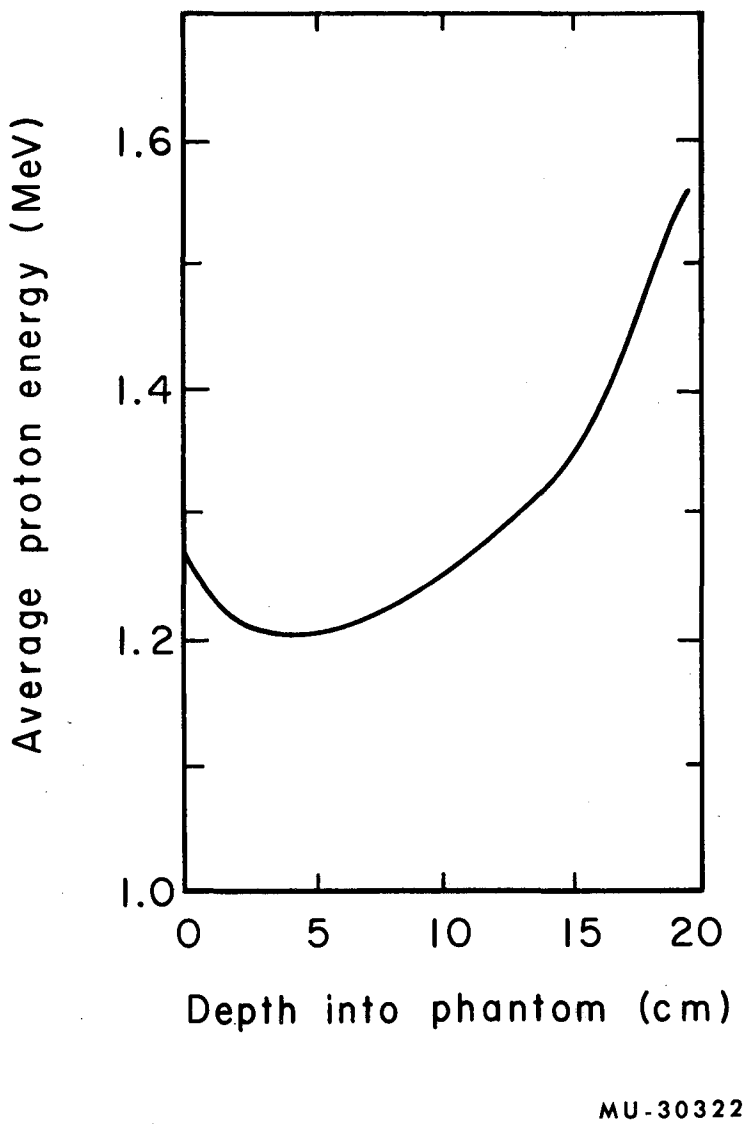

Fig. 11. Variation of mean recoil proton energy with depth into phantom, excluding thermal (n, p) tracks from incident PuBe neutrons.

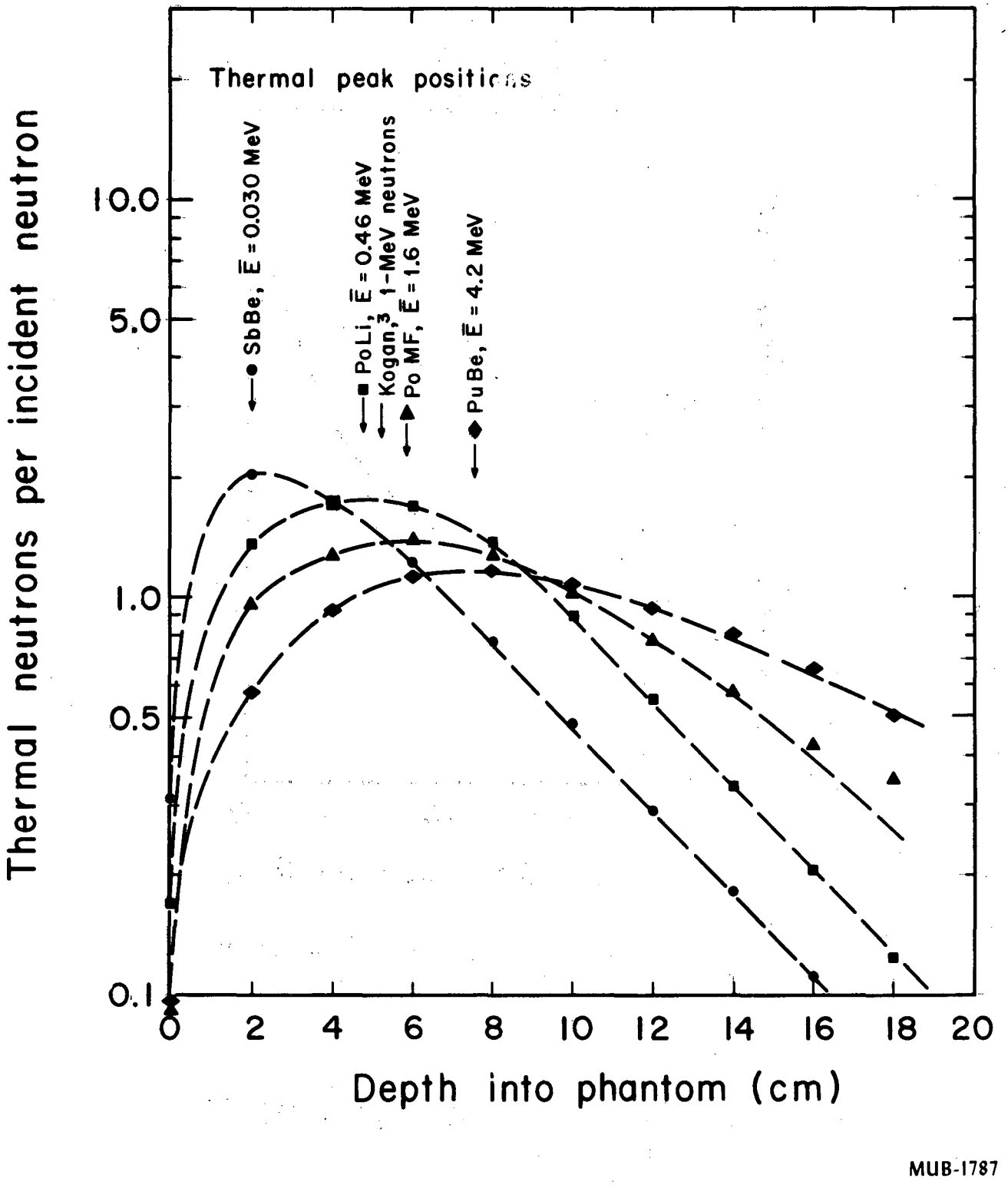

Fig. 12. Thermal-neutron flux per incident neutron with depth into phantom corrected for $1/r^2$.

half of the phantom. This dose depression is, in part, due to the insensitivity of the emulsions to low-energy neutrons. Furthermore, the emulsions were scanned by the "random walk" system. Track lengths are measured by a three-dimensional scanner, going from the terminal point of a measured track to the nearest neighboring track ending. Thus the probability of measuring a short track which may appear as little more than a point is considerably less than the probability of detecting a longer track with two end points to offer. Although a correction was made for these low-energy omissions, it may not have been sufficient for the larger proportion of neutrons in the region towards the front of the phantom.

B. Slow Neutrons

The tissue-dose components due to the exothermic capture reactions in nitrogen and hydrogen are calculated directly from the thermal-neutron flux measured by the indium foils and BF_3 detector. The regular behavior of the thermal distribution (thermal neutrons/fast neutron) within the phantom is noteworthy. Figure 12 presents results that might have been predicted for normally incident monoenergetic neutrons comparable to the mean energies of the point sources used. Flux measurements made at varying source-phantom distances indicate that the $1/r^2$ correction made for geometric attenuation is a logical assumption for the distribution behavior within the phantom, for comparison with parallel-beam conditions. Figure 13 shows the thermal peak depth into the phantom as a function of energy or mean energy of the indicated neutron sources. The present results show fair agreement of complex-spectra peak depth with peak depths of calculated and experimental parallel-beam monoenergetic neutrons.

1. $N^{14}(n,p)C^{14}$

The tissue-dose component for the capture reaction in nitrogen is directly proportional to the measured thermal-neutron flux at the dose site. Included in the calculation are the reaction cross sections at 0.025 eV, 1.75; atomic density of nitrogen, 1.72×10^{21} atoms/cm^3; and a proton recoil energy of 0.63 MeV:

$$\text{rads} = (1.72\times10^{21})\times(0.63)\times(1.75\times10^{-24})\times(1.6\times10^{-8}) = 3.034\times10^{-11}\,\text{n}^{-1}\text{cm}^2.$$

The resultant dose in rads per unit incident flux (rads per n/cm^2) is shown in Figs. 14 to 17. One can readily see that there is generally good agreement between these results and those of Smith and Boot, who used gold foils and monoenergetic beams.[7] Some differences may be explained by the fact that the present study used an atomic density for nitrogen in tissue of 1.72×10^{21}, compared with 1.29×10^{21} for Smith's work, and a proton recoil energy of 0.63 MeV was used here compared with Smith's value of 0.62 MeV.

The distribution pattern from PuBe neutrons shows the dose at the back surface to be 91% of the dose delivered to the front surface of the phantom, with the maximum dose occurring at a depth of 7.7 cm in the phantom. The position of the peak dose from the front surface seems to vary logarithmically as the mean energy of the neutron sources (Fig. 13). The positions of the peak $N^{14}(n,p)C^{14}$ dose for Po mock fission, PoLi, and SbBe neutrons

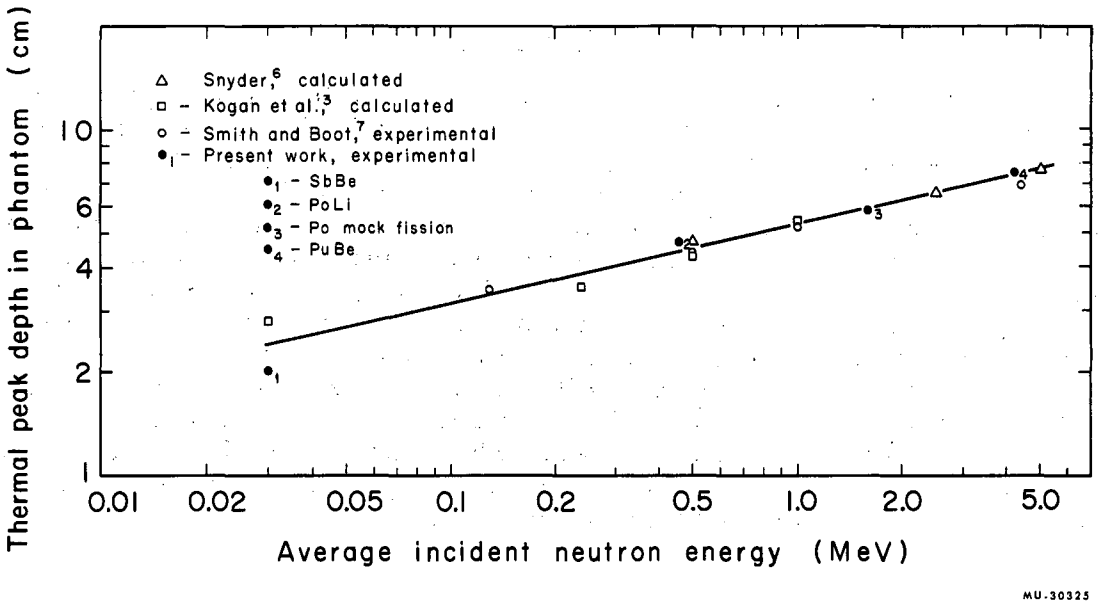

Fig. 13. Thermal-neutron flux peak depth into phantom as a function of incident neutron energy.

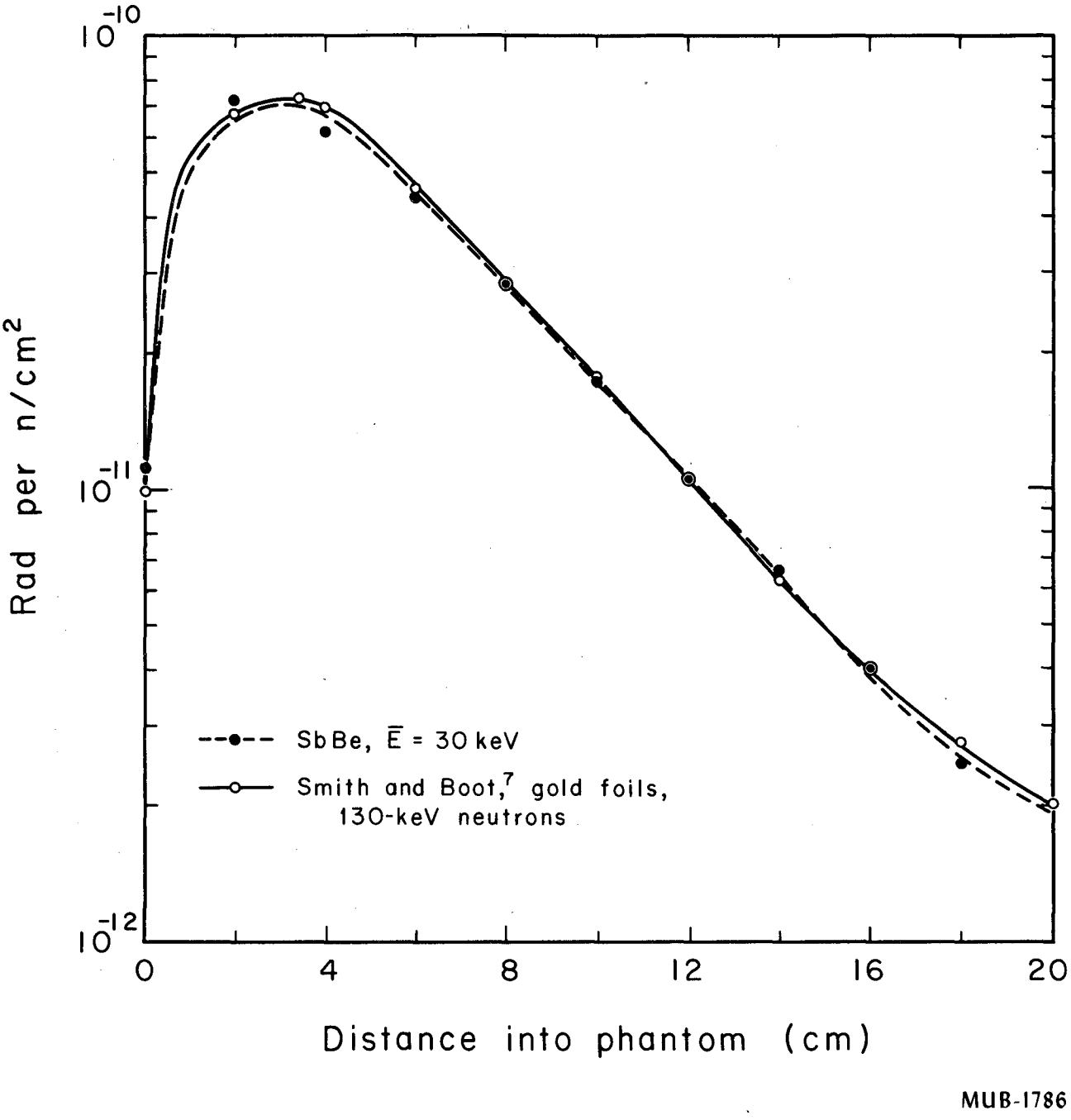

Fig. 14. $N^{14}(n, p)C^{14}$ depth-dose curves for SbBe.

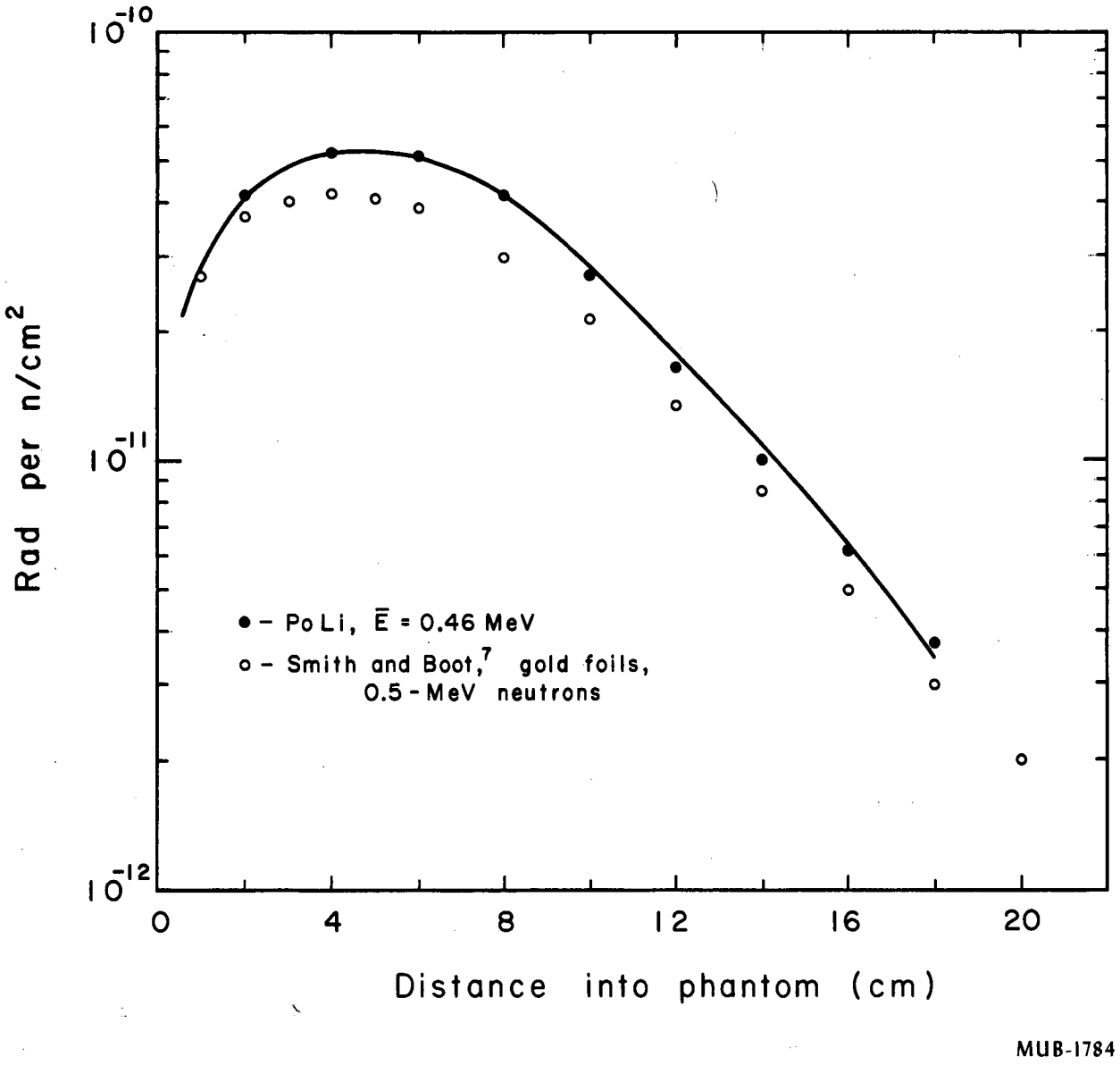

Fig. 15. $N^{14}(n, p)C^{14}$ depth-dose curves for PoLi.

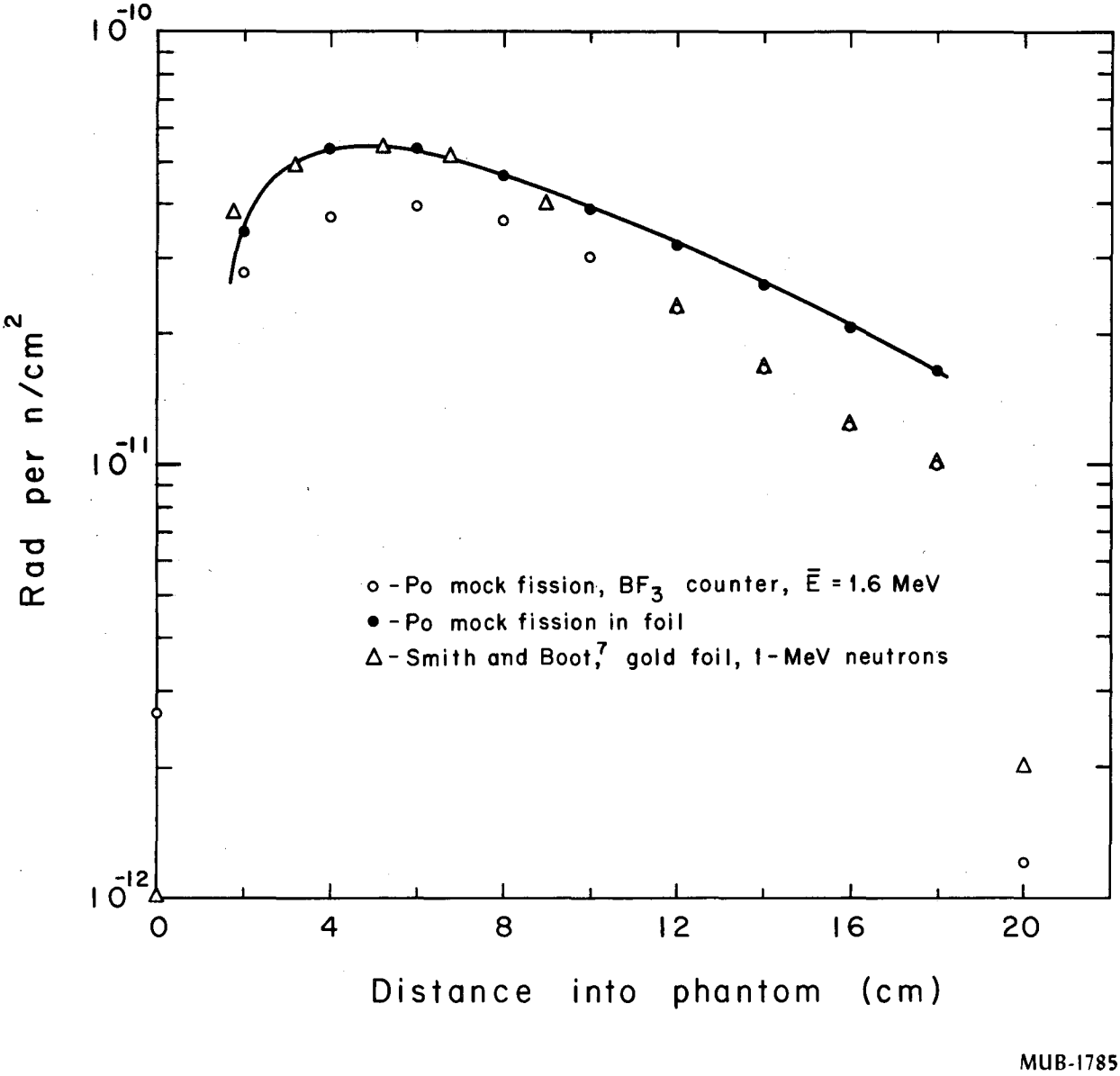

Fig. 16. $N^{14}(n, p)C^{14}$ depth-dose curves for Po mock fission.

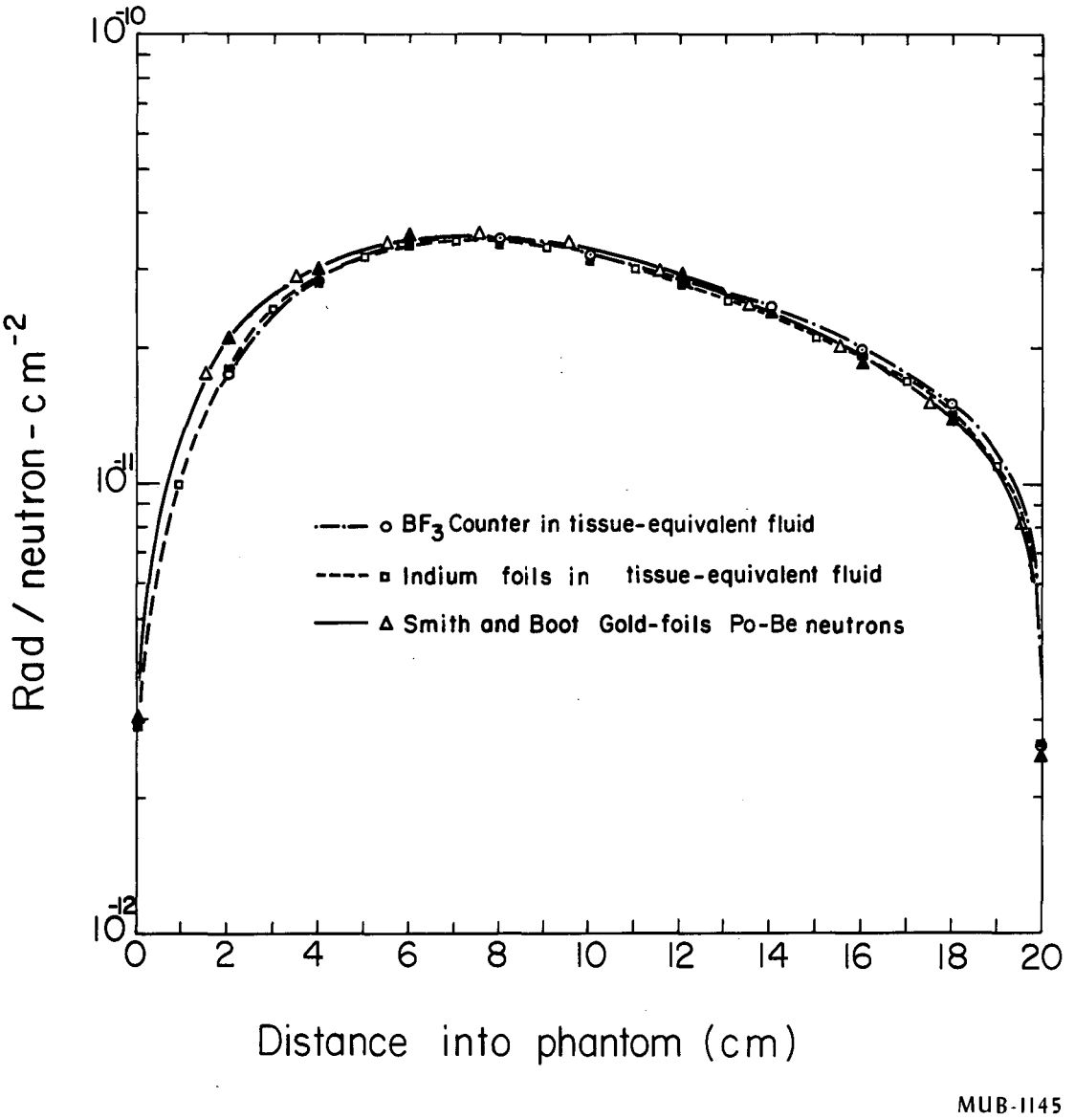

Fig. 17. $N^{14}(n, p)C^{14}$ depth-dose curves for PuBe neutrons.

impinging on the front surface of the phantom are 5.8, 4.8, and 2 cm, respectively. The corresponding ratios of front-to-back readings are 46, 40, and 17%.

2. $H^1(n,\gamma)H^2$

Because the mean free path of the γ quanta released in neutron capture by hydrogen is 22 cm in tissue, most of the γ dose at any point arises from neutron capture in a volume external to the one under consideration. The phantom was therefore treated as a series of disks 1 cm thick and 36 cm in diameter, normal to the external source. The gamma dose was calculated according to the formula of Taylor,[11] by using each hypothetical disk as a plane circular isotropic monoenergetic source within the phantom, and by integrating numerically to yield the total dose at any depth. Thus the γ dose not only depends upon the magnitude and position of the thermal-flux peak, but also upon the rate at which the thermal flux falls off within the phantom. The γ-dose peak will not necessarily coincide with the thermal peak.

According to Taylor's formula, the dose per unit time from any slab at a distance z from the slab is

$$D_z = KS_z\phi_{th}F(z) \qquad \text{(see Appendix C).}$$

For the $H^1(n,\gamma)H^2$ reaction in tissue, $K = 4.45\times10^{-10}$ rad per γ/cm^2, ϕ_{th} is the absolute thermal flux within the slab, and F(z) is a function of the distance from the slab—this function employs energy-absorption buildup factors and first-order exponential integrals. The source strength S_z—in terms of photons per cm^2 of a given slab—was obtained by the use of the capture cross section at 0.025 eV of 0.33 b and an atomic hydrogen density of 5.98×10^{22} atoms/cm^3. Then

$$S_z = (0.33\times10^{-24})\times(5.98\times10^{22}) = 1.973\times10^{-2}\ \gamma \text{ per } n/cm^2.$$

The results are shown in Figs. 18 to 20. The γ dose shows close agreement with the results of Smith and Boot[7] who used relatively monoenergetic sources of energies close to the mean energy of the present sources, their results being, in general, slightly higher than the broad spectrum dose. The $N^{14}(n,p)C^{14}$ dose, calculated from the same thermal-flux values, shows a closer agreement with Smith and Boot's value. This is due to the difference in nitrogen abundance used in the two studies, which indicates that lower slow-flux values were obtained in our work.

Although Kogan, who did not use buildup factors, employed a γ-distribution calculation less precise than the formula of Taylor, his resultant dose does not differ greatly from Taylor's calculation for a similar flux. Figure 15, a comparison of Kogan's calculated $H^1(n,\gamma)H^2$ dose with his reported thermal-flux values applied to Taylor's formula, indicates close agreement near the front of the phantom but a more rapid drop toward the back. This accounts in part for the difference in shape of Kogan's results but, more important, indicates a real variance in Kogan's thermal-neutron distribution from that of the other investigators.

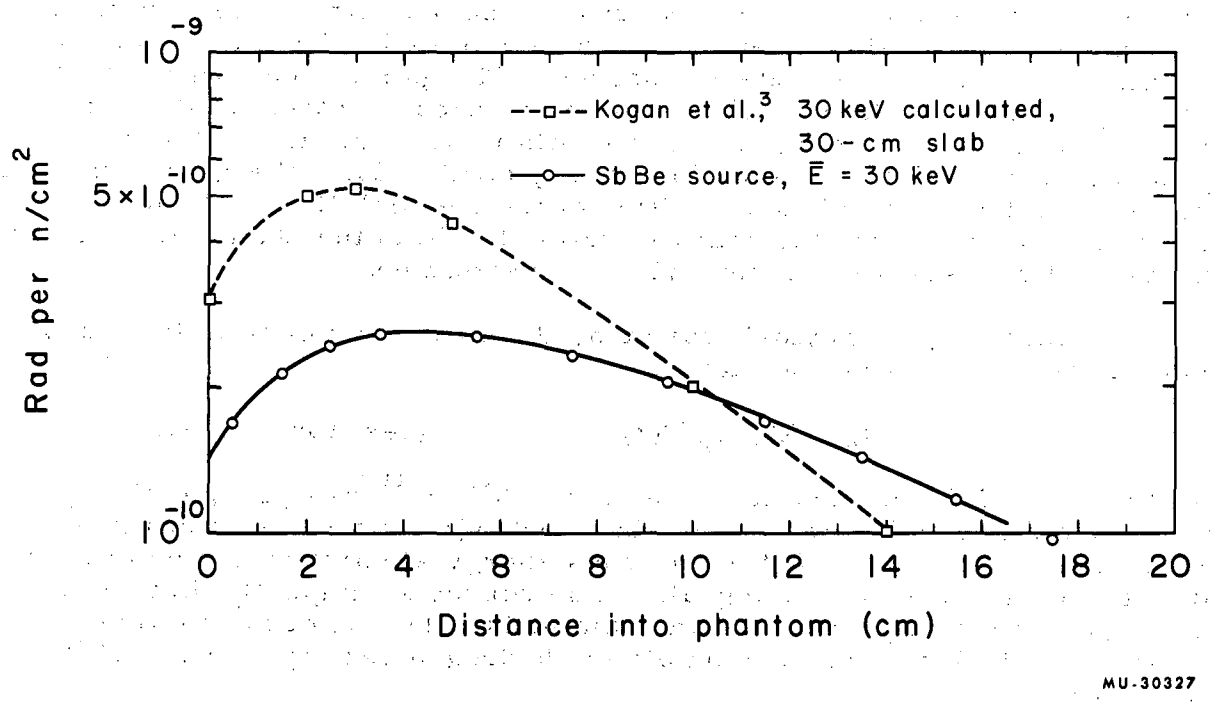

Fig. 18. $H^1(n, \gamma)H^2$ depth-dose curves for SbBe.

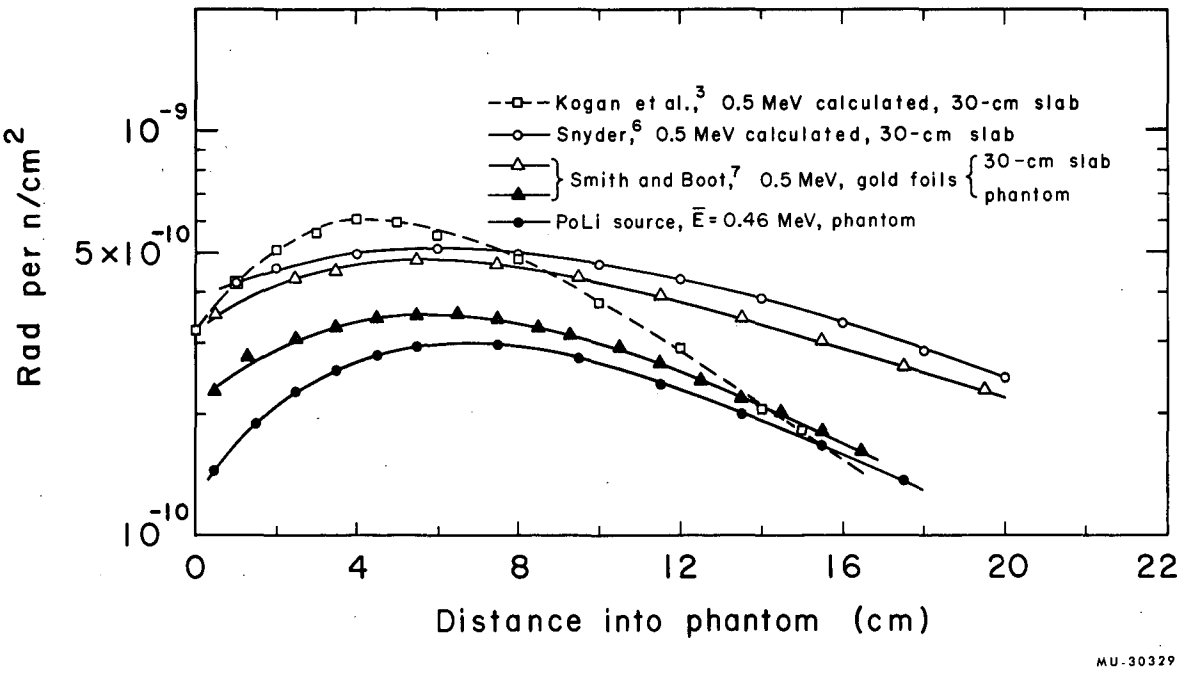

Fig. 19. $H^1(n, \gamma)H^2$ depth-dose curves for PoLi.

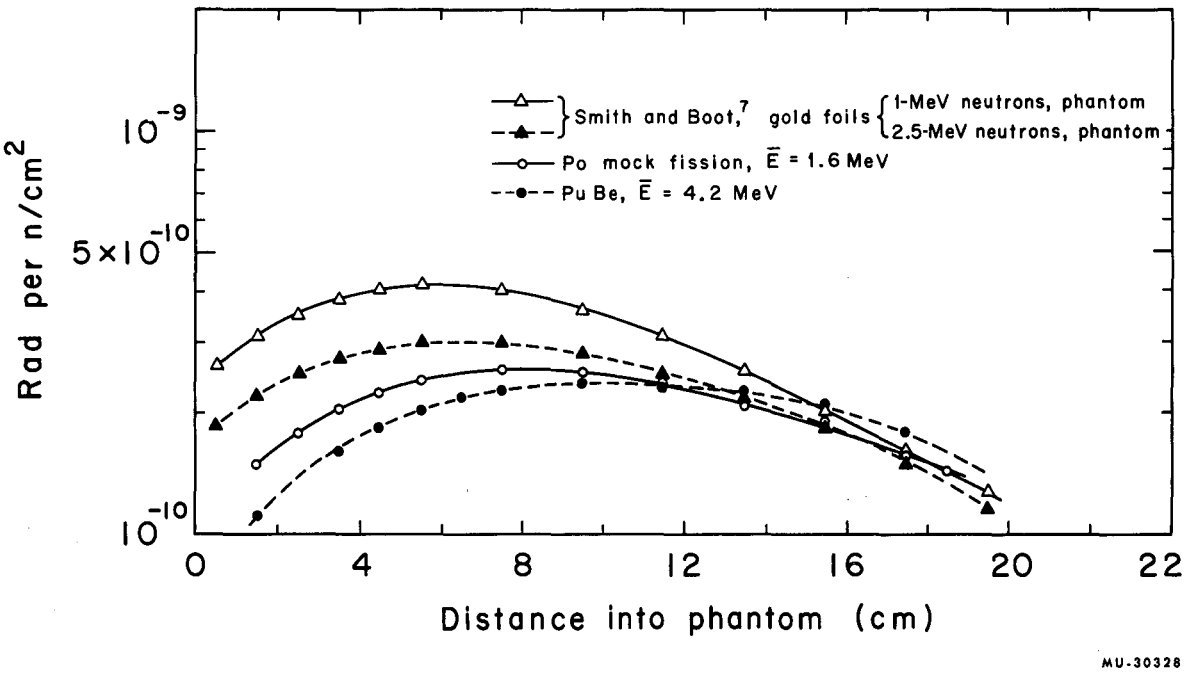

Fig. 20. $H^1(n, \gamma)H^2$ depth-dose curves for Po mock fission, PuBe neutrons.

Snyder's calculations on an infinite slab yield higher results than the present work (Fig. 19), but the difference probably arises from the choice of models. It is likely that both will overestimate the actual dose because of the added source volume imposed when approximating an elliptical cylinder by a series of uniform circular slabs.

IV. CONCLUSION

The components of the neutron tissue dose resulting from exposure to point sources of broad spectrum width exhibit favorable similarities to previously reported calculated and experimentally determined depth-dose curves for monoenergetic neutrons under parallel-beam conditions. Although the absolute magnitude of the present doses appear to be slightly less than those reported by Snyder and Neufeld,[6] and Smith and Boot,[7] the respective variations with depth show good agreement when the incident flux is adjusted by a $1/r^2$ geometry correction.

The thermal distribution within the phantom exhibited behavior similar to monoenergetic sources of neutron energy equivalent to the average energies of the (α, n) and (γ, n) sources, with respect to thermal peak positions, magnitude, and depth-distribution behavior.

ACKNOWLEDGMENTS

The authors wish to thank: Mr. H. Wade Patterson and Dr. Roger Wallace for their assistance and support which made the project possible; Mr. William Robison and Dr. Hiroaki Akagi for their continuous assistance during the early stages of the program; Mr. William Wadman for his greatly appreciated help with the neutron sources; Mr. Richard Lehman and the staff of the Health Physics Department for their cooperation and helpful discussions.

The authors especially wish to thank Mr. Lloyd D. Stephens for the many hours he has unselfishly given to the project.

This work was done under the auspices of the U. S. Atomic Energy Commission.

APPENDIX A. FLUX-DEPRESSION-FACTOR CALCULATION

The depression of thermal-neutron flux at the point of measurement by the indium foil was calculated by using Bothe's formula and thermal diffusion constants for water as given by Tittle.[9] The foil is treated as a spherical shell, assuming that a disk of radius R is approximately equivalent to a spherical shell of radius 2R/3. The flux depression by which the measured thermal-neutron flux must be multiplied is

$$F_{th} = 1 + \alpha/2 \left[\frac{3R}{2\lambda_{tr}} \cdot \frac{L}{R+L} - 1 \right] ,$$

where

$R = 1.27$ cm,

λ_{tr} = transport mean free path in tissue = 0.425 cm,

L = thermal diffusion length in tissue = 2.76 cm.

The average probability of absorption, α, of a neutron by a layer of thickness d is

$$\alpha = 1 - e^{-\mu d}(1-\mu d) + \mu^2 d^2 \; E_i(-\mu d) ,$$

where

$d = 9.2 \times 15^2$ gm/cm^2 ,

μ = absorption coefficient $= \frac{N_0 \sigma}{A} = 9.07 \times 10^{-1}$ cm^2/gm ,

$E_i(-\mu d)$ = exponential integral function.

Thus, for the flux depression by indium foils in tissue, $F_{th} = 1.15$.

APPENDIX B. CALIBRATION OF INDIUM FOILS IN CONCRETE CAVITY

In calculating the slow-neutron dose, the cross sections for the particular reactions involved were taken for thermal energies of 0.025 eV. Thus it is necessary to make certain assumptions about the neutron spectra in the region of 0.025 eV in order that the spectra may be properly weighted with respect to the variance of both the detector and tissue cross sections in this region. The calibration of the slow-neutron detectors were made by using the slow-neutron flux created by a fast-neutron source placed in a concrete cavity. From the strength of the fast-neutron source, the thermal-neutron flux within the cavity may be estimated, independent of the source spectrum:

$$\text{thermal flux} = 1.25\, Q/S,$$

where Q is the source strength in neutrons/sec, and S is the inner surface area of the cavity.[8] Because of the 1/v dependence of the indium cross section

and the high resonance peak at 1.5 eV, the calibration would be accurate only if the thermal-epithermal region of the spectrum were the same as the corresponding energy region within the phantom.

Shielding the indium foils with cadmium allows a determination of the thermal-region flux (that region below the indium resonance peaks) and the resonance-region flux both in the phantom and in the cavity because of the rapid drop in the cadmium absorption just prior to the indium peaks. A comparison of the ratio of thermal activation to "resonance" activation in the cavity to the thermal-resonance ratio at various depths in the phantom allows a better interpretation of the thermal calibration of the bare-foil measurements based on the cavity standard (Fig. 21). The ratio measurements were made with 0.005-in. foils, 26 cm^2, wrapped around a thin-walled Geiger tube to approximate 50% geometry.[9] Under these conditions the thermal flux is given by $\phi_{th} = C(A - 1.07 A_{cd})$, where A and A_{cd} are the saturated activities of the bare and cadmium-covered foils, respectively, corrected to a foil mass of 2.42, and C is a constant. The thermal-resonance ratio is just

$$\frac{\phi_{th}}{\phi_{res}} = \frac{A - A_{cd}}{1.07 A_{cd}} .$$

In a sense, the neutrons in the resonance region are being neglected, which is valid if one assumes approximately 1/v dependence of the dose reaction cross sections. Measurements in the phantom made with a BF_3 counter covered with a cadmium sheet were negligible compared to bare BF_3 measurements; furthermore, the strict 1/v behavior of the BF_3 counter gives a reputable estimation of the relative tissue absorption in the thermal and epithermal regions. All foil measurements in the phantom were compared to BF_3 measurements under identical conditions, and showed very close agreement.

The thermal-resonance ratio taken in the cavity was 3.3:1, while the ratio in the phantom was found to vary with depth, ranging from 7.4:1 to 15:1, depending upon the position in the phantom. This would indicate that the final tissue dose results would be minimal, although somewhat compensated by the error introduced by the assumption of strict 1/v dependence of the tissue reaction cross sections.

APPENDIX C. GAMMA-DOSE CALCULATION

The gamma dose resulting from the exothermic capture reaction in hydrogen was calculated by the exact formula of Taylor.[11] The phantom was imagined to be a series of disks 1 cm thick and 36 cm in diameter; each disk was treated as a plane monoenergetic source of uniform isotropic distribution. The dose rate at a distance z from a particular slab of radius R is

$$D_z = f \frac{S_z \phi_{th}}{2} \left(A_1 \left\{ E_1[(1+a_1)\mu_0 z] - E_1[(1+a_1)\mu_0 z \sqrt{1+(R/z)^2}] \right\} + (1 - A_1) \left\{ E_1[(1+a_2)\mu_0 z] - E_2[(1+a_2)\mu_0 z \sqrt{1+(R/z)^2}] \right\} \right) ,$$

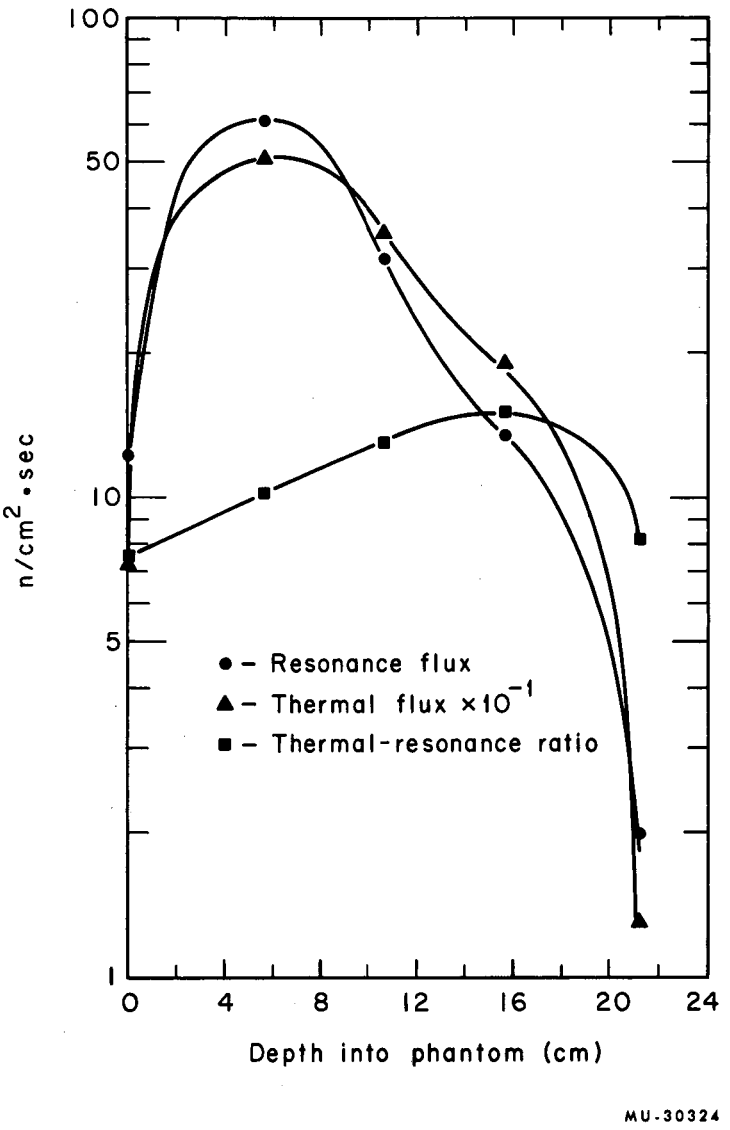

Fig. 21. Thermal-resonance neutron flux relationship with depth in phantom.

where

S_z = source strength = 1.973×10^{-2} γ per n/cm^2,

ϕ_{th} = thermal-neutron flux at source,

f = conversion factor from flux to dose, taking μ, the mass energy absorption coefficient for 2.226-MeV gamma energy, as 0.025 cm^{-1}; f = $(8.904)(10)^{-10}$ rad per γ/cm^2,

μ_0 = narrow-beam attenuation coefficient = 0.046 cm^{-1},

A_1, a_1, and a_2 are Taylor's values for energy absorption buildup factors in water: 7.3, -0.0650, and 0.0488, respectively,

$E_1(x) = \int_x^\infty \frac{e^{-\xi}}{\xi} d\xi$, a first-order exponential integral.

The values of D_z for a particular point in the phantom are numerically integrated to yield the total dose for that depth. The self-dose of a slab source is shown by Smith and Boot[7] to be the dose at $z = 1/3$ cm.

REFERENCES

1. Enrico Fermi, Nuclear Physics, revised edition (University of Chicago Press, Chicago, 1950).

2. E. Tochilin and S. Ross, Radiation Res. 7, 158 (1956).

3. A. M. Kogan, G. G. Petrov, L. A. Chudov, and P. A. Yampol'skii, The Neutron Tissue Dose, Soviet J. At. Energy (English Transl.) 7, 830 (1961).

4. B. J. Moyer (Lawrence Radiation Laboratory, Berkeley), private communication.

5. B. J. Moyer, Survey Methods for Neutron Fields, University of California Radiation Laboratory Report UCRL-1635, January 1952 (unpublished).

6. Walter S. Snyder and J. Neufeld, Calculated Depth Dose Curves in Tissue for Broad Beams of Fast Neutrons, Brit. J. Radiol. 28, 342 (1955).

7. J. W. Smith and S. J. Boot, The Variation of Neutron Dose with Depth in a Tissue Equivalent Phantom, Phys. in Med. Biol. 7, 45 (1962)(unpublished).

8. R. L. Lehman and H. Akagi, Neutron Dosimetry in and Around Human Phantoms by Use of Nuclear Track Emulsion, Lawrence Radiation Laboratory Report UCRL-9967 Rev., June 1962 (unpublished).

9. C. W. Tittle, Slow Neutron Detection by Foils, Nucleonics 9, 60 (1951).

10. H. W. Patterson and R. Wallace, A Method of Calibrating Slow Neutron Detectors, University of California Radiation Laboratory Report UCRL-8359, July 1958 (unpublished).

11. J. J. Taylor, Application of Gamma-Ray Build-Up Data to Shield Design, Westinghouse Electric Corp. Report WAPD-RM-217, 1954 (unpublished).